

PAPER

Perfect-absorption graphene metamaterials for surface-enhanced molecular fingerprint spectroscopy

To cite this article: Xiangdong Guo *et al* 2018 *Nanotechnology* **29** 184004

View the [article online](#) for updates and enhancements.

Perfect-absorption graphene metamaterials for surface-enhanced molecular fingerprint spectroscopy

Xiangdong Guo^{1,2,3,4}, Hai Hu^{1,3}, Baoxin Liao^{1,3}, Xing Zhu^{1,2,4}, Xiaoxia Yang^{1,3,5} and Qing Dai^{1,3,5} 

¹ Division of Nanophotonics, CAS Center for Excellence in Nanoscience, National Center for Nanoscience and Technology, Beijing, 100190, People's Republic of China

² Academy for Advanced Interdisciplinary Studies, Peking University, Beijing, 100871, People's Republic of China

³ University of Chinese Academy of Sciences, Beijing 100049, People's Republic of China

⁴ State Key Lab for Mesoscopic Physics, School of Physics, Peking University, Beijing 100871, People's Republic of China

E-mail: yangxx@nanoctr.cn and daiq@nanoctr.cn

Received 12 December 2017, revised 1 February 2018

Accepted for publication 19 February 2018

Published 9 March 2018



CrossMark

Abstract

Graphene plasmon with extremely strong light confinement and tunable resonance frequency represents a promising surface-enhanced infrared absorption (SEIRA) sensing platform. However, plasmonic absorption is relatively weak (approximately 1%–9%) in monolayer graphene nanostructures, which would limit its sensitivity. Here, we theoretically propose a hybrid plasmon-metamaterial structure that can realize perfect absorption in graphene with a low carrier mobility of $1000 \text{ cm}^2 \text{ V}^{-1} \text{ s}^{-1}$. This structure combines a gold reflector and a gold grating to the graphene plasmon structures, which introduce interference effect and the lightning-rod effect, respectively, and largely enhance the coupling of light to graphene. The vibration signal of trace molecules can be enhanced up to 2000-fold at the hotspot of the perfect-absorption structure, enabling the SEIRA sensing to reach the molecular level. This hybrid metal-graphene structure provides a novel path to generate high sensitivity in nanoscale molecular recognition for numerous applications.

Supplementary material for this article is available [online](#)

Keywords: perfect absorption, metamaterials, graphene plasmon, surface enhanced spectroscopy

(Some figures may appear in colour only in the online journal)

1. Introduction

Infrared (IR) spectroscopy is a fast and non-destructive method for identifying chemicals, with widespread applications in chemical detection [1], food safety [2], bio-sensing [3] and other fields [4–7]. It is difficult to detect nanoscale molecules with IR spectroscopy due to the large mismatch between mid-IR wavelengths (from 2.5 to 25 μm) [8] and molecular dimensions (<10 nm). Surface-enhanced IR absorption (SEIRA) using graphene plasmons can largely

enhance the light-molecule interaction and directly detect nanoscale molecules [5, 7, 9, 10]. Graphene plasmons can confine IR light in three dimensions, at scales that are over 100 times smaller than its free space wavelength, corresponding to an approximately 10^6 -fold smaller volume [11]. Furthermore, graphene plasmons can be dynamically tuned by electrostatic gating to selectively probe IR vibrational fingerprints over a wide IR spectral range [7, 12]. Thus, graphene plasmons have become a promising candidate for SEIRA applications.

The sensitivity of SEIRA is closely related to the plasmon absorption, according to the coupled harmonic oscillator model

⁵ Authors to whom any correspondence should be addressed.

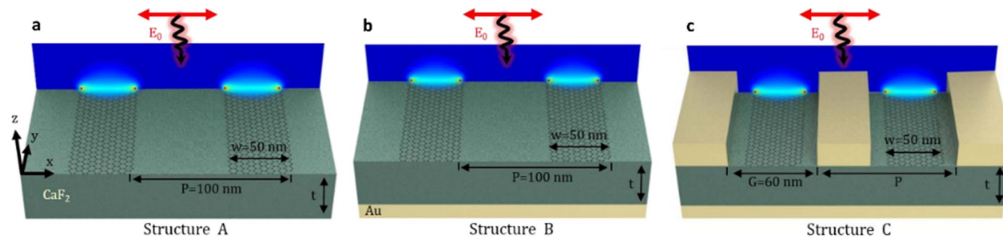


Figure 1. Schematic of three graphene plasmon structures. (a) Structure A, graphene ribbon array. Periodicity $P = 100$ nm, ribbon width $W = 50$ nm and CaF_2 thickness t varied. (b) Structure B, evolved from structure A with a 50 nm thick gold film at the bottom. (c) Structure C, evolved from structure B with a gold optical grating added between the graphene nanoribbons. The thickness and gap (G) of the gold grating are both 60 nm. IR plane wave incidence is from the z direction, with the electric field polarized in the x direction. The graphene ribbons and gold grating are unlimited in the y direction. The E_z distributions in graphene are overlapped on graphene plasmonic ribbons in the back panels.

[13]. However, the plasmonic absorption of monolayer graphene is relatively weak; for example, the experimentally measured absorption is usually 1%–9% in the IR range [14–17]. In addition to the effects of large momentum mismatch between graphene plasmons and free space light, the relatively low carrier mobility in graphene nanostructures largely decreases the plasmon strength [18, 19]. Chemical vapor deposited graphene is usually patterned and etched into nanostructures via oxygen plasma etching to excite localized plasmons. Defects and impurities introduced by the device fabrication processes and substrates (e.g., SiO_2) largely degrade the carrier mobility of graphene in these nanostructures (generally less than $1000 \text{ cm}^2 \text{ V}^{-1} \text{ s}^{-1}$). The measured plasmon absorption of fabricated graphene nanostructures (1%–9%) is much lower than simulated values (as high as 20%–75%) based on high-quality graphene with a mobility of approximately $10\,000 \text{ cm}^2 \text{ V}^{-1} \text{ s}^{-1}$ [19, 20].

Here, we propose a kind of perfect absorption structure of graphene plasmon with easily achievable mobility ($1000 \text{ cm}^2 \text{ V}^{-1} \text{ s}^{-1}$) to enhance its light–matter interaction. Gold grating and reflector are integrated in the metamaterials which can focus IR light on the graphene nanostructures due to its strong reflection and scattering [20–22]. The perfect absorption is achieved by combining the high light coupling quantum efficiency of graphene [5–7], large field enhancement in the gaps of gold grating [21–24] and the interference effect introduced by the back reflector [20, 25]. The maximum absorption and electric field intensity enhancement are calculated to reach 99% and 4 orders of magnitude, respectively. This high field enhancement results in ultrasensitive SEIRA, as theoretically demonstrated by trace SO_2 gas ($<1.2 \times 10^{-13} \text{ mol m}^{-3}$ molecular dipoles' density) with signal enhancement at the hotspot of about 2000-fold. This work provide a promising plat form for practical implementations of ultrasensitive SEIRA.

2. Structural design and physical mechanism

The perfect absorption structure of graphene plasmons with a low carrier mobility combines the contribution of both a back reflector and a metal grating. To illustrate their functions, we comparatively study three types of structures: pristine graphene ribbon arrays (structure A), graphene ribbon arrays

with a gold reflector (structure B) and graphene ribbon arrays with both a gold reflector and a gold grating (structure C), as shown in figure 1. In this study, we adopt a graphene structure that is widely used in experiments: a periodic array of graphene nanoribbons with a ribbon width W of 50 nm and a 1:2 width-to-pitch ratio (structure A). First, we optimize the graphene plasmonic absorption (GPA) of the back reflector by tuning the thickness of the CaF_2 substrate (structure B). A CaF_2 film (with a refractive index $n_{\text{CaF}_2} = 1.22$ in the IR range) [26, 27] is used because it can serve as a gate dielectric and as a transparent substrate in the IR spectral region [5, 28]. Then, we insert a periodic gold grating into the gap of the graphene ribbons to further enhance the graphene plasmonic strength (structure C).

The graphene plasmons are simulated by employing the finite element method. The simulation model employs periodic boundary condition to simplify the hybrid nanostructures. For modeling the graphene, there are two type of approaches in previous research papers [29, 30]. The graphene can be treated as a surface boundary condition (2D approach), which has no physical thickness. Another approach (3D approach) is also valid by modeling the graphene as 1 nm or 0.335 nm thickness volume material. In previous literature, the calculated results are nearly consistent by using two different approaches [29]. Here, the 3D approach is adopted. Graphene is modeled as a material with a finite thickness and an equivalent relative permittivity that depends on thickness [31, 32]. The equivalent relative permittivity ϵ_g is derived from the surface conductivity σ of the graphene, calculated by $\epsilon_g = 1 + i\sigma/\epsilon_0\omega t_g$, where ϵ_0 is the permittivity of free space, ω is the angular frequency of the incident light and t_g is the graphene layer thickness. Here, to save computing time and storage space, t_g is not the real thickness (~ 0.34 nm) and is set to 1 nm [33]. The mesh size of graphene is 0.1 nm and the mesh size gradually increases outside the graphene layer, at which the calculations reach proper convergence. The surface conductivity of graphene, σ , is calculated from the Kubo formula, which consists of interband and intraband transitions. In the mid- and far-IR regions, the intraband transitions dominate. At room temperature ($T = 300$ K), which satisfies the requirement of $k_B T \ll E_f$, the complex surface conductivity can be

approximately calculated from the Drude model [34–36]:

$$\sigma = \frac{ie^2 E_f}{\pi \hbar^2 (\omega + i/\tau)}, \quad (1)$$

where e is the electron charge, E_f is the doped graphene Fermi energy, \hbar is the reduced Planck constant and K_B is the Boltzmann constant. The graphene Fermi energy can be tuned by electrical gating or chemical doping, offering an active way to control optical properties. The relaxation time τ is defined as $\tau = \mu E_f / e v_f^2$, where $v_f = c/300$ is the Fermi velocity and $\mu = 1000 \text{ cm}^2 \text{ V}^{-1} \text{ s}^{-1}$ is the carrier mobility of graphene.

In the simulation, the metallic mirror and grating are made of gold, with an optical permittivity (near- and mid-IR) described by the simple Drude model [37, 38]:

$$\varepsilon(\omega) = 1 - \frac{\omega_p^2}{\omega^2 + i\omega\gamma}, \quad (2)$$

where $\omega_p = 1.32 \times 10^{16} \text{ rad s}^{-1}$ is the plasma frequency and $\gamma = 1.2 \times 10^{14} \text{ rad s}^{-1}$ is the damping frequency (or Drude relaxation rate).

3. Results and discussion

The absorption spectra of pristine graphene nanoribbons (structure A) with different CaF_2 thickness are displayed in figure 2(a). The resonance frequency occurs at 1333 cm^{-1} , and the absorption strength is slightly affected by the thickness of the CaF_2 film, which was varied from 10% to 15%. This absorption may be larger than the experimentally obtained values because the experimental effective ribbon-to-pitch ratios are much smaller than $1/2$, due to the 28 nm non-electric-conducting edges [14]. After coating with a gold film, we study the enhancement of the graphene plasmons by the reflector (structure B). The reflector has the same graphene plasmon resonance frequency ($\omega_p = 1333 \text{ cm}^{-1}$), while the absorption strength varies significantly. In this Salisbury screen structure, the Fabry–Perot interference effect occurs, and the thickness of the CaF_2 film becomes a key factor. Absorption spectra for CaF_2 films of various thicknesses are displayed in figure 2(b). As shown, the absorption strength changes from 5% to 52% as the CaF_2 film thickness varies from 0.3 to $1.5 \mu\text{m}$. Compared with structure A, structure B with the proper dimensions can largely increase the plasmon absorption (>4 times).

The effects of CaF_2 film thickness on the graphene plasmon strength in structures A and B are compared in figure 2(c). The resonant absorption (RABs) results are both periodic with the thickness of the CaF_2 film in structures A and B, and here, we plot around the half period. The critical thickness values are approximately $t_1 = 1.53 \mu\text{m}$ and $t_2 = 3.06 \mu\text{m}$ for both structures. However, the structures exhibit opposite maximum and minimum absorption (i.e., π -phase shift). At $t_1 = 1.53 \mu\text{m}$, the RABs of structure B reaches the maximum value (approximately 52%), while structure A reaches a minimum of absorption

(approximately 10%). The RABs minimum of structure B occurs at $t_2 = 3.06 \mu\text{m}$ (approximately 5%), which is even lower than that of structure A. The interference theory of light explains this phenomenon, and details can be found in the Supporting Information. Briefly, periodic RABs occurs because of interference of the reflected light from the top and bottom surfaces of the CaF_2 film (figure S1 is available online at stacks.iop.org/NANO/29/184004/mmedia). In structure A, half-wave loss (π -phase change) only occurs after the light reflection at the top surface of the CaF_2 film, when the light is incident from an optically thinner medium (air) to an optically denser medium (CaF_2). In structure B, the half-wave loss occurs twice, with light reflections at both the top and bottom surfaces of the CaF_2 film, when the light is incident from air/ CaF_2 to CaF_2/Au . This difference explains the π -phase shift between structures A and B. The interference conditions are further supported by the critical CaF_2 film thickness, where t_1 and t_2 are approximately equal to $t(\lambda_p/4) = \lambda_p/(4n_{\text{CaF}_2}) = 1.537 \mu\text{m}$ and $t(\lambda_p/2) = \lambda_p/(2n_{\text{CaF}_2}) = 3.074 \mu\text{m}$. Thus, with a proper CaF_2 film thickness, the reflected light loss in structure B can be suppressed. The efficiency of graphene absorption can be improved by approximately 5-fold when the CaF_2 film thickness is approximately $1.53 \mu\text{m}$.

Although the reflector layer has increased the graphene plasmon absorption from approximately 10%–52%, the absorption is still far from perfect. This phenomenon is a direct result of the high plasmon damping rate, Γ_p , at low mobility, as illustrated in the Supporting Information. We calculate several absorption spectra for structure B with different graphene mobilities, as shown in figure S2. When the carrier mobility increases to $5000 \text{ cm}^2 \text{ V}^{-1} \text{ s}^{-1}$, perfect absorption can almost be achieved in structure B, which is in accordance with previous studies [25]. The plasmon damping rate, Γ_p , which can be extracted from the plasmon resonance linewidth Γ via $\Gamma_p = \Gamma/2\hbar$ [14, 15], increases significantly as the mobility decreases. The scattering, such as inelastic scattering with phonons and elastic carrier scattering processes, increased with decreasing mobility. Hence, the absorption intensity is reduced by large plasmon damping.

We introduce a gold grating with the lightning-rod effect to further improve the graphene absorption with the interference effect, as in structure C. Absorption spectra for varied periodicity are plotted in figure 2(d), with fixed values of $G = 60 \text{ nm}$, $W = 50 \text{ nm}$, and $t = 1.53 \mu\text{m}$. The absorption gradually increases as the periodicity increases from 100 to 250 nm and then decreases as the period increases from 250 to 400 nm, as shown in figure 2(d). The RABs values are extracted and plotted as a function of the periodicity in the inset of figure 2(d). The RABs values can reach nearly 100% at a periodicity of 250 nm.

For SEIRA applications, we more closely consider the component absorbed by the graphene plasmons than the total absorption in the as-obtained perfect-absorption structure. We calculate the contributions of graphene and others (gold and CaF_2) to the total absorption in structure C as follows. The power dissipation density (W m^{-3}) in graphene is expressed

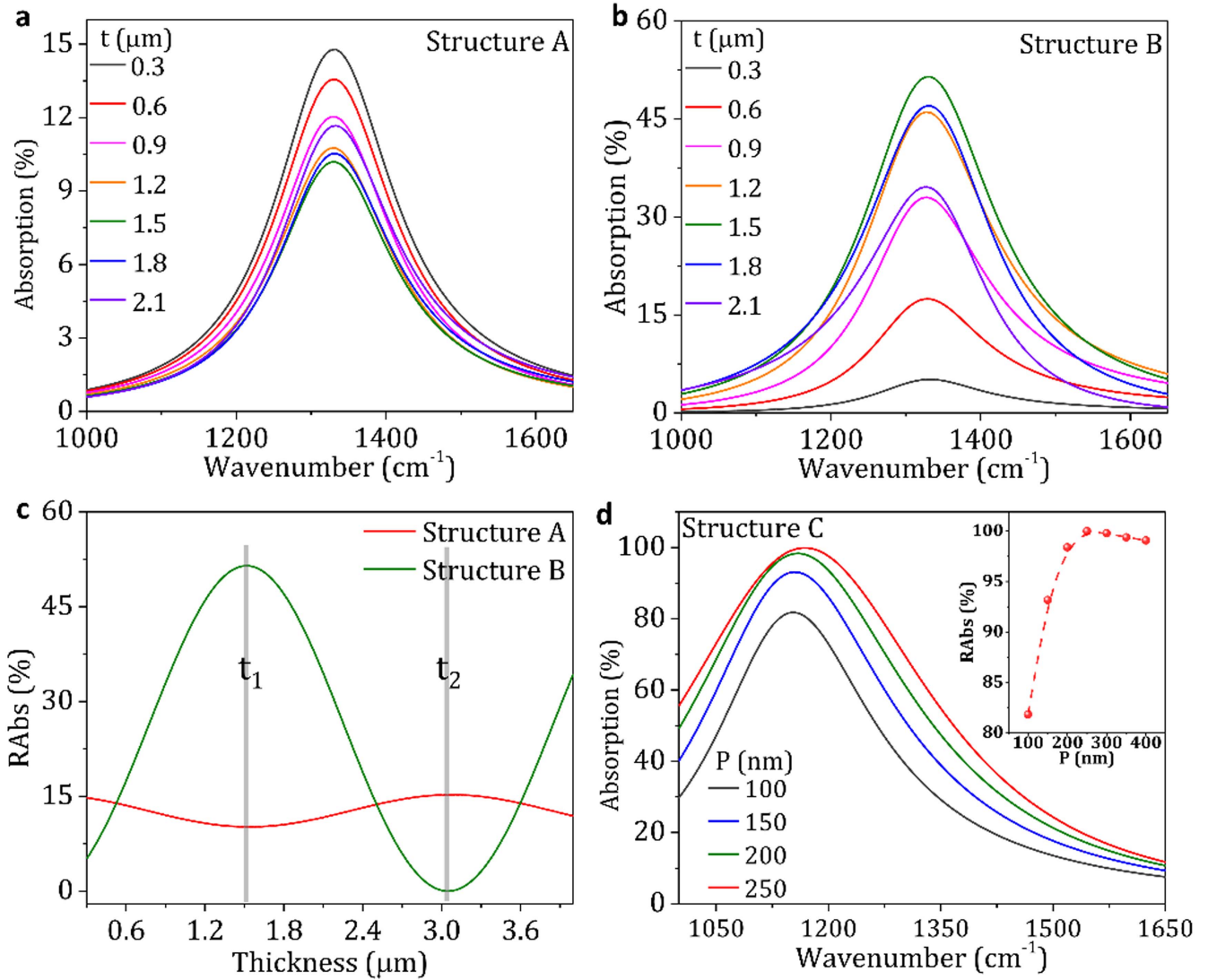


Figure 2. Calculated absorption spectra in the A, B and C structures. (a), (b) Absorption spectra of structures A and B with the CaF₂ thickness varied from 0.3 to 2.1 μm, respectively. (c) RAbs strength extracted from (a) to (b) plotted as a function of CaF₂ thickness. (d) Absorption spectra of structure C with the periodicity varied from 100 to 250 nm. Inset: RAbs strength extracted from (d) as a function of the periodicity. The graphene Fermi energy is 0.3 eV in all structures.

as [39, 40]

$$w = \frac{1}{2} \varepsilon_0 \omega \varepsilon''(\omega) |E|^2, \quad (3)$$

where E is the strength of the near electric field and $\varepsilon''(\omega)$ is the imaginary part of the graphene dielectric function. Then, the absorption can be calculated by the ratio equation, where the total absorbed power within a volume, V , to the incident power through the exposed surface area S is as follows [39, 40]:

$$A' = \frac{\iiint w dV}{\frac{1}{2} c_0 \varepsilon_0 |E_{inc}|^2 S}, \quad (4)$$

where the denominator is the Poynting vector in the surface area. For structure C, as discussed here, volume integration is carried out in the x and z directions only, and the y

dimensional length is canceled out. Due to the periodicity in the x direction, the integration length can be set to a period, that is, S is set equal to P . According to (4), the GPA in structure C is calculated and plotted in figure 3(a). The GPA can reach approximately 99% in the perfect-absorption structure, while the other absorptions are near 1%, as calculated by the difference between the total absorption and the GPA. Thus, the GPA in this perfect-absorption structure is one order of magnitude larger than the pristine GPA in structure A at low graphene mobility ($1000 \text{ cm}^2 \text{ V}^{-1} \text{ s}^{-1}$).

According to (3), the GPA is closely connected to the electric field intensity of the graphene plasmon, which also directly determines light-matter interactions. The electric field intensity distributions of graphene plasmons in structures A, B and C are plotted. In the simulation, we just consider the classical model. The graphene ribbons edges have almost no quantum finite-size effects [41, 42]. At the graphene plasmon resonance frequency, the electric field distributions of

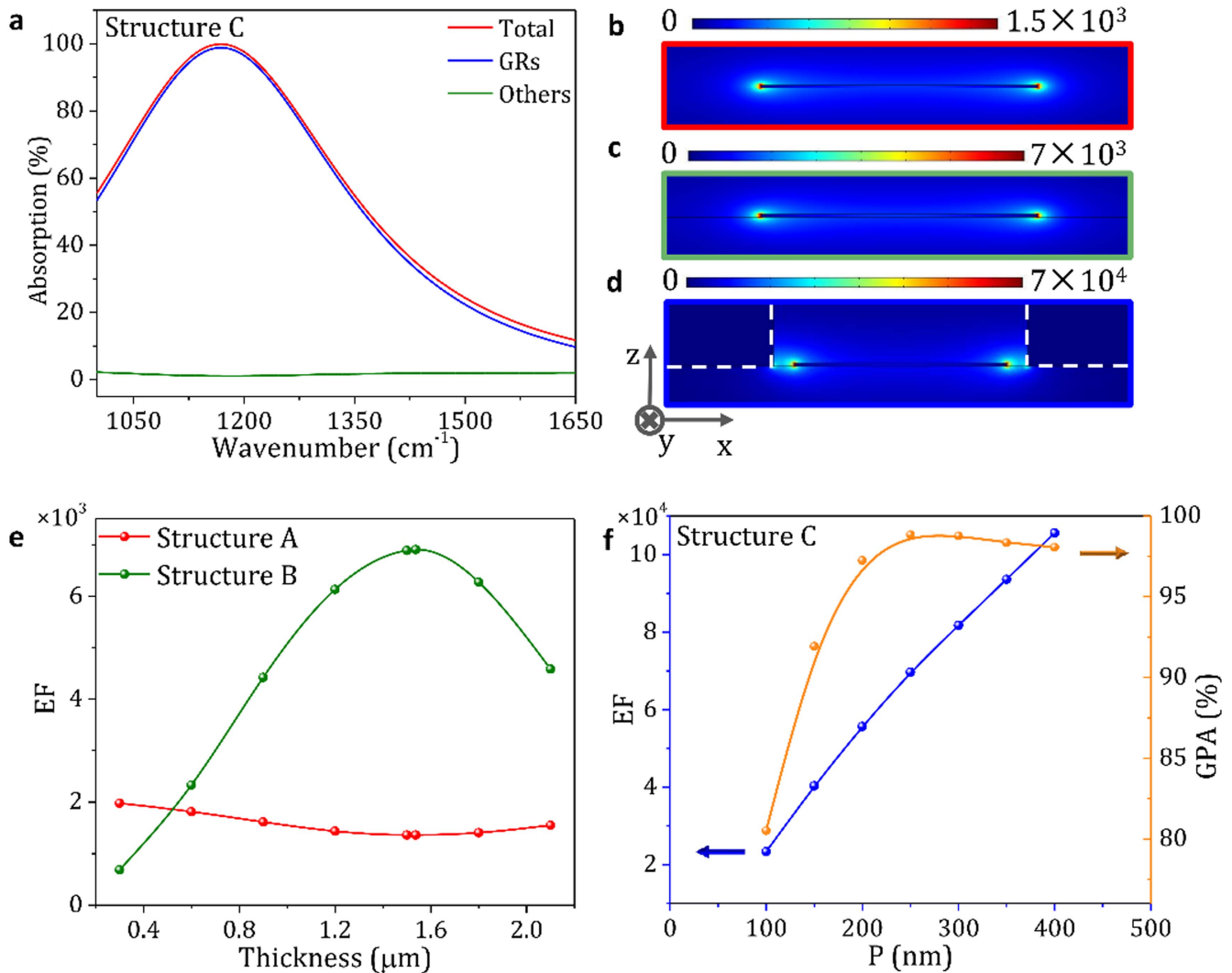


Figure 3. (a) Absorption of each component under perfect absorption conditions in structure C with a periodicity of 250 nm. Red curve: total absorption. Blue curve: graphene ribbon absorption (GPA). Green curve: other absorption. The superposition of the blue and green curves results is shown by the red curve. (b)–(d) Simulated electric field distribution (x – z plane) for the graphene ribbon at the plasmon resonance frequency in structures A (b), B (c) and C (d). Color bars indicate the electric field intensity enhancement factor $EF = (E/E_0)^2$. (e) The EF of structures A and B, respectively, for CaF₂ films of varied thickness. (f) EF (blue line) and GPA (orange line) for structure C with varied periodicity.

structures A, B, and C are similar, and the field hotspots are located along the edges of the graphene nanoribbons. The enhancement factor (EF) (7×10^3) of structure B occurs at a substrate thickness of a quarter wavelength and is approximately 4.7-fold higher than the EF (1.5×10^3) of structure A. The EF (7×10^4) of structure C, which has perfect absorption, is enhanced by one order of magnitude compared to that of structure B. The enhancement of the electric field intensity of graphene plasmons is similar to that of the absorption spectrum. This result is further supported by the periodic variation of EF with CaF₂ film thickness in structures A and B, as shown in figure 3(e), which have the same variation tendencies as the RAbs spectra in figure 2(c). However, the EF in structure C increases monotonically as the periodicity gradually increases for a fixed gap ($G = 60$ nm), as displayed in figure 3(f), which is not consistent with the variation of the RAbs spectra in figure 2(d), which we further discuss below.

The resonant GPA is affected by the EF of the graphene plasmon and also depends on the duty cycle (W/P) of the graphene ribbons with different periodicity P and fixed W . The varied periodicity (P) is used to calculate the GPA in the denominator of equation (4). The change in GPA with the periodicity is plotted in figure 3(e), and the maximum GPA is approximately $P = 250$ nm, which agrees well with the maximum total absorption of the whole structure. Meanwhile, the strong GPA, rather than the total absorption, plays a key role in the application of SEIRA. Hence, the perfect IR absorption and huge electric field intensity enhancement have inherent advantages in the SEIRA technique, which can directly provide chemical information about trace analytes by probing characteristic molecular fingerprints.

The huge EF in structure C can be understood by the lightning-rod effect in addition to the enhancement of the reflector. The physical nature of the lightning-rod effect is

metallic screening, which prevents the electric field from penetrating the perfect metal [43]. The expulsion of the electric field from the interior of the metal nanostructures improves the electric field EF in the gaps between the metals. At the large wavelength region, the screening effect of the metal is obvious because the real part of the dielectric function becomes large and negative. Thus, in the mid-IR range, the electric field focuses on the gap of the gold grating, which improves the excitation efficiency of the graphene ribbon plasmons and enhances the graphene near electric field. Thus, as the P/G ratio increases, the expulsion of the electric field from the interior of the gold grating becomes more concentrated at the gap. A plane-parallel capacitor is formed by the gap.

The large EF in the perfect-absorption structure C implies great performance for SEIRA applications. To test the performance, trace SO_2 gas is used as an example of a target analyte. Since SO_2 gas is a toxic fume, it must be detected to ensure public health and environmental safety. SO_2 has two S–O vibrational modes at $\sim 1351 \text{ cm}^{-1}$ (labeled as M) and $\sim 1375 \text{ cm}^{-1}$ (labeled as N) in the IR fingerprint range. Figure 4(a) shows the experimentally measured IR spectrum (black circles) and an analytical model based on summing Lorentz oscillators, which are used for fitting as follows [44, 45]:

$$\varepsilon(\omega) = \varepsilon_\infty + \sum_{n=1}^N \frac{e^2 N_n / (\varepsilon_0 m_e)}{\omega_n^2 - \omega^2 - i\gamma_n \omega}, \quad (5)$$

where ε_∞ is a constant dielectric background, N_n is the volume density of molecular dipoles, e is the electron charge, m_e is the electron rest mass, ω_n is the molecular vibrational frequency and γ_n is the molecular damping. In the simulation, we suppose that the weak absorption data are generated by the 8 nm thick free-standing SO_2 molecular layer. We find that the following set of parameters gives good agreement with the experimental absorption data. The extracted parameters for modes M and N are $\varepsilon_\infty = 1$, $N_M = 2.7 \times 10^{-13} \text{ mol m}^{-3}$, $\omega_M = 1351 \text{ cm}^{-1}$, $\gamma_M = 183 \text{ cm}^{-1}$, $N_N = 1.2 \times 10^{-13} \text{ mol m}^{-3}$, $\omega_N = 1375 \text{ cm}^{-1}$, and $\gamma_N = 77 \text{ cm}^{-1}$.

These three structures are comparatively studied in depth for molecular sensing. We select the SO_2 layer exhibiting a weaker IR absorption by one order of magnitude, as shown in figure 4(a), as the analyte. The absorption values of pristine molecular vibrational modes M and N are approximately 0.032% and 0.039%, respectively, which are hardly distinguishable (figure 4(b)). However, the vibrational modes M and N are present as obvious dips in the plasmon RAs peaks. The dips originate from Fano coupling between the graphene plasmons (dashed lines) and vibrational modes, where destructive interference occurs. The depth of the Fano resonance reveals the coupling strength between the vibrational modes and the graphene plasmons. To directly demonstrate the coupling effect, the depths are extracted and plotted in figure 4(c), which demonstrates the difference between the structure absorption with and without molecules (namely, delta absorption). As shown, the delta absorption successively

increases from structures A to B and C. The molecular signal enhancement is calculated as the ratio between the delta absorption and the pristine molecular absorption, which are plotted in figure 4(d). The enhancements of modes M and N are increased from 48-fold and 32-fold in structure A to 415-fold and 355-fold in structure C. The enhancements of modes M and N in structure C are approximately 9-fold and 11-fold more than that in structure A, respectively. This trend is entirely consistent with the IR absorption values of these structures, where the IR absorption value of structure C is approximately 10 times that of structure A.

As another feature, the vibrational mode signal close to the graphene plasmon resonance peak is enhanced more than the wing signals. For example, the absorption of mode M is lower than that of mode N in the pristine molecular absorption spectrum, but the delta absorption of mode M is even larger than that of mode N in all structures (figure 4(c)). This result occurs because the frequency of mode M is closer to the plasmon resonance frequency than that of mode N , and the near-field strength is higher at that frequency. The plasmonic resonance linewidths Γ of the three structures are also extracted and plotted in figure 4(d). As observed, Γ of structure C is approximately twice that of structures A and B. In particular, structure C has realized near-perfect absorption ($>95\%$) of wide-range IR light ($\sim 100 \text{ cm}^{-1}$ spectral width) in graphene nanoribbons. The broad absorption peak of structure C can overlap and enhance molecular fingerprint vibrational modes over a wider spectrum range. This wide range and the high enhancement efficiency, which is approximately one order of magnitude greater than that of the traditional graphene structure A, make the perfect-absorption structure C a promising candidate for next-generation molecular fingerprint sensors.

The average molecular signal enhancement of SO_2 calculated from far-field IR spectra is an average over the whole unit cell. However, the plasmonic field enhancement is strongly concentrated at the ribbon edges, and the EF at the ribbon edges (hotspots) should be substantially larger than the average EF. Thus, we use a SO_2 patch (8 nm thick along the x and z directions) as a local molecular probe and place it at different positions along the graphene ribbon. First, we study the SEIRA enhancement across the nanoribbon. The center of the SO_2 patch is moved along the x -axis from $x = 0$ to $x = -21 \text{ nm}$, while the height is fixed at $z = 5 \text{ nm}$. The absorption spectra at different x positions are shown in figure 5(b). The Fano dips of the M and N modes become more obvious as the SO_2 patch is moved closer to the graphene ribbon edge. The local molecular signal enhancement is calculated and plotted in figure 5(c). The local molecular signal enhancement of mode M is still larger than that of mode N , which is in agreement with the average enhancement, as shown in figure 4. The enhancements both increase significantly as the SO_2 patch position is moved closer to the ribbon edge and reach the maximum enhancement (approximately 2000-fold) at the edge, which is approximately 3 times higher than the local molecular signal enhancement at the ribbon center and approximately 5 times higher than the average

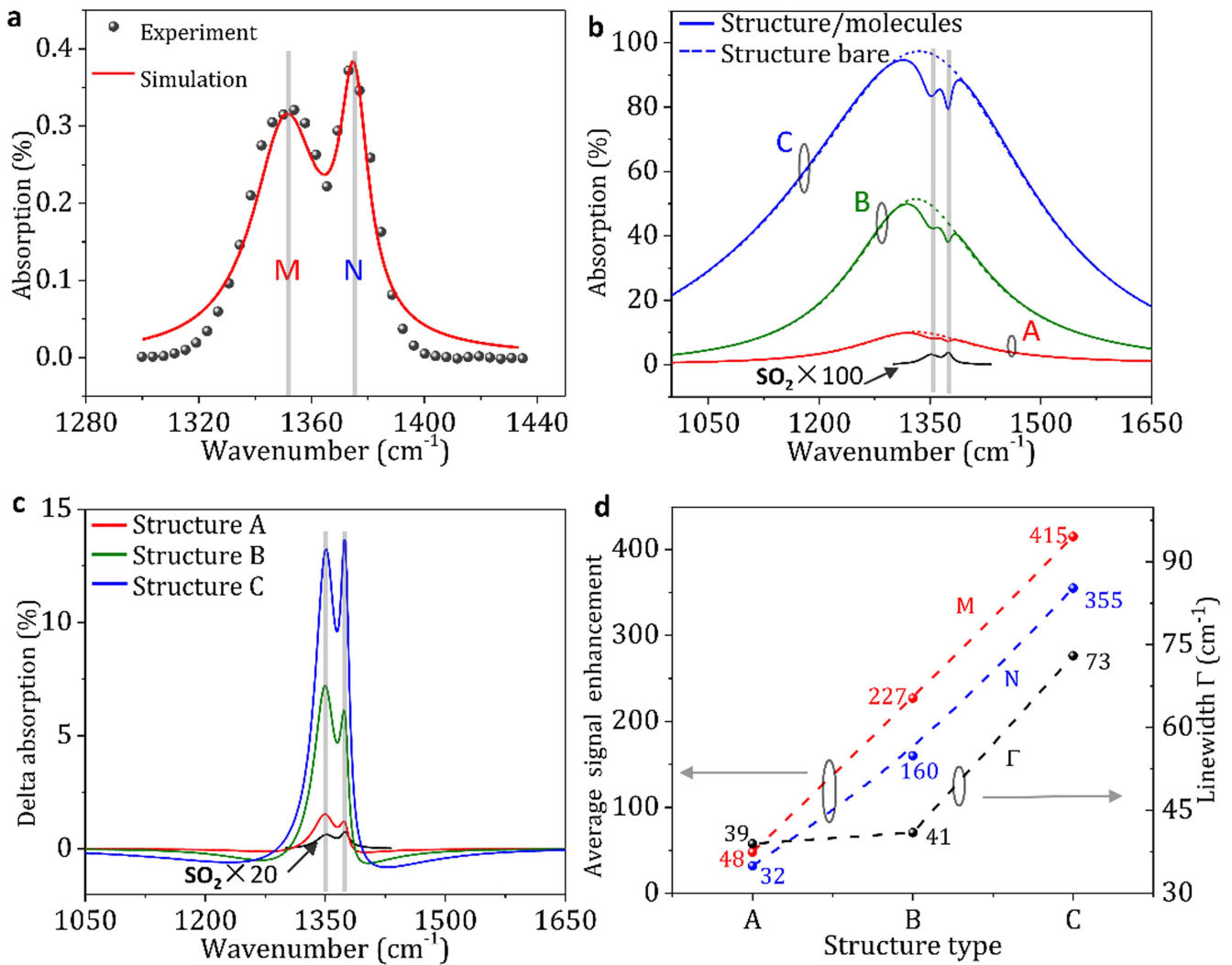


Figure 4. (a) Absorption spectra of SO_2 obtained from an analytical model compared with experimental data (black circles). Two fingerprint vibrational modes of SO_2 ($M \sim 1351 \text{ cm}^{-1}$, $N \sim 1375 \text{ cm}^{-1}$) are considered. (b) Absorption spectra of graphene plasmons in structures A (red curves), B (green curves) and C (blue curves) before (dashed lines) and after (solid lines) application of an 8 nm thick SO_2 layer coating. An enlarged (100-fold) absorption spectrum of the SO_2 layer is plotted (black line). (c) Plasmon-enhanced M and N mode responses extracted from (b). Pristine SO_2 absorption for comparison (black line). (d) Signal enhancements (delta absorption of structures/pristine molecular vibrational absorption) of all structures are displayed. To avoid detuning between the graphene plasmon resonance frequency and the vibrational frequency, we adjusted the graphene E_f to 0.375 eV in structure C.

enhancement. The change in local molecular signal enhancement values is primarily determined by the local electromagnetic field enhancement. Thus, we extract the near-field EF from $x = 0$ to -25 nm with $z = 5 \text{ nm}$ in figure 5(c). These data follow a trend similar to that of the local molecular signal enhancement of modes M and N , with a dramatic decrease from $x = -25$ to -10 nm followed by a relatively small value in the ribbon center region. The slight difference between these tendencies is generated by the uneven electromagnetic field in the SO_2 patch region. We also investigate the variation of SEIRA enhancement along the z direction with fixed $x = -21 \text{ nm}$ (graphene edge). The absorption spectra for different z positions are shown in figure S2, and the local molecular signal enhancement is calculated and plotted in figure 5(d). The local molecular signal enhancement of modes M and N is also consistent with the near-field EF, which is calculated as a function of the z position based on the near-field distribution (black line

in figure 5(d)). The EF decreases exponentially with the z distance, and the local molecular signal enhancement also decreases largely as the z distance increases. Thus, the enhanced SEIRA signal primarily originates from molecules located at the hotspots (graphene ribbon edges). The local signal enhancement of hotspots is considerably larger than the average enhancement, which can be used to detect smaller numbers of molecules. Alternatively, the molecules act as a probe for the near field and thus provide an elegant way to obtain information about the near-field distributions of plasmonic structures.

4. Conclusions

In summary, we have presented a hybrid plasmonic meta-material to realize perfect absorption on deteriorated graphene, which can focus the mid-IR light on the graphene

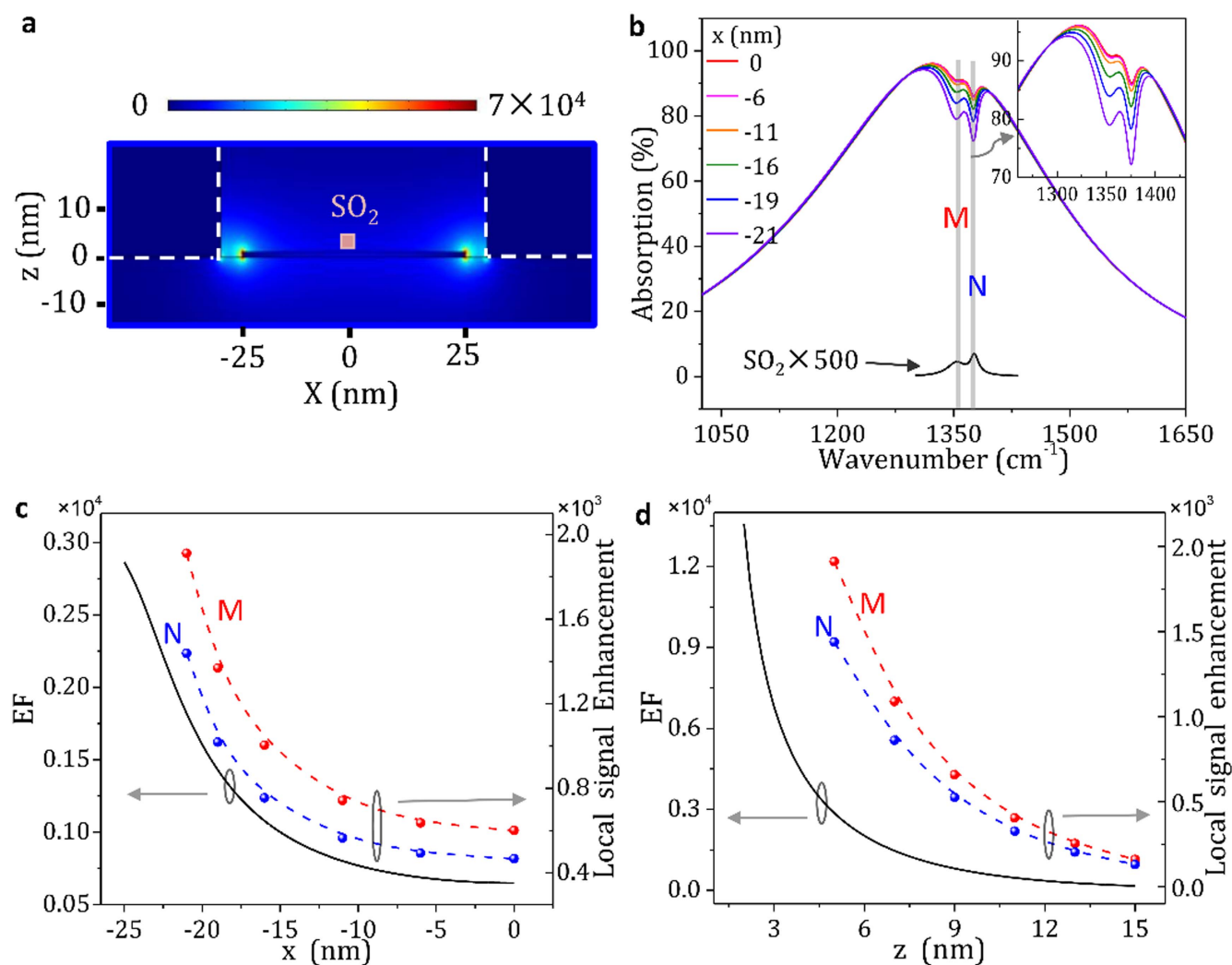


Figure 5. (a) Simulated electric field distribution of structure C with graphene $E_f = 0.375$ eV. The position of the SO_2 molecule patch is indicated. (b) Absorption spectra of structure C with the SO_2 molecule patch located at different positions along the x -axis. The dips are enlarged in the inset. An enlarged absorption spectrum of the SO_2 patch is also shown. (c) Near-field intensity EF (black line) and local molecular signal enhancement of modes M and N as a function of the x position with fixed $z = 5$ nm. (d) Near-field intensity EF (black line) and local molecular signal enhancement of modes M and N as a function of the z position at the graphene ribbon edge.

nanostructures by gold reflector and grating and then largely enhance the GPA. It can increase the graphene absorption by one order of magnitude. By exploiting the electrically tunable perfect-absorption structure in vibrational fingerprint spectra, it can probe the S–O vibrational mode of trace SO_2 molecules with the large absorption signal enhancement at the hotspot (approximately 2000-fold). Therefore, our proposed perfect IR absorption structures provide a promising method for realizing ultrasensitive molecular fingerprint sensors.

Acknowledgments

This work was supported by the National Basic Key Research Program of China (Grant No. 2015CB932400), the National Key Research and Development Program of China (Grant No. 2016YFA0201600), the National Natural Science Foundation of China (Grant Nos. 51372045, 11504063 and 11674073), and

the key program of the Bureau of Frontier Sciences and Education Chinese Academy of Sciences (QYZDB-SSW-SLH021).

ORCID iDs

Qing Dai  <https://orcid.org/0000-0002-1750-0867>

References

- [1] Bagri A, Mattevi C, Acik M, Chabal Y J, Chhowalla M and Shenoy V B 2010 Structural evolution during the reduction of chemically derived graphene oxide *Nat. Chem.* **2** 581–7
- [2] Mauer L J, Chernyshova A A, Hiatt A, Deering A and Davis R 2009 Melamine detection in infant formula powder using near- and mid-infrared spectroscopy *J. Agric. Food Chem.* **57** 3974–80
- [3] Garczarek F and Gerwert K 2006 Functional waters in intraprotein proton transfer monitored by FTIR difference spectroscopy *Nature* **439** 109–12

- [4] Neubrech F, Huck C, Weber K, Pucci A and Giessen H 2017 Surface-enhanced infrared spectroscopy using resonant nanoantennas *Chem. Rev.* **117** 5110–45
- [5] Hu H, Yang X, Zhai F, Hu D, Liu R, Liu K, Sun Z and Dai Q 2016 Far-field nanoscale infrared spectroscopy of vibrational fingerprints of molecules with graphene plasmons *Nat. Commun.* **7** 12334
- [6] Li Y, Yan H, Farmer D B, Meng X, Zhu W, Osgood R M, Heinz T F and Avouris P 2014 Graphene plasmon enhanced vibrational sensing of surface-adsorbed layers *Nano Lett.* **14** 1573–7
- [7] Rodrigo D, Limaj O, Janner D, Etezadi D, de Abajo F J G, Pruneri V and Altug H 2015 Mid-infrared plasmonic biosensing with graphene *Science* **349** 165–8
- [8] Hu H et al 2017 Large-scale suspended graphene used as a transparent substrate for infrared spectroscopy *Small* **13** 1603812
- [9] Amenabar I et al 2013 Structural analysis and mapping of individual protein complexes by infrared nanospectroscopy *Nat. Commun.* **4** 2890
- [10] Brown L V, Zhao K, King N, Sobhani H, Nordlander P and Halas N J 2013 Surface-enhanced infrared absorption using individual cross antennas tailored to chemical moieties *J. Am. Chem. Soc.* **135** 3688–95
- [11] Low T and Avouris P 2014 Graphene plasmonics for terahertz to mid-infrared applications *ACS Nano* **8** 1086–101
- [12] Brar V W, Jang M S, Sherrott M, Lopez J J and Atwater H A 2013 Highly confined tunable mid-infrared plasmonics in graphene nanoresonators *Nano Lett.* **13** 2541–7
- [13] Adato R, Artar A, Erramilli S and Altug H 2013 Engineered absorption enhancement and induced transparency in coupled molecular and plasmonic resonator systems *Nano Lett.* **13** 2584–91
- [14] Yan H, Low T, Zhu W, Wu Y, Freitag M, Li X, Guinea F, Avouris P and Xia F 2013 Damping pathways of mid-infrared plasmons in graphene nanostructures *Nat. Photon.* **7** 394–9
- [15] Yang X, Zhai F, Hu H, Hu D, Liu R, Zhang S, Sun M, Sun Z, Chen J and Dai Q 2016 Far-field spectroscopy and near-field optical imaging of coupled plasmon-phonon polaritons in 2D van der Waals heterostructures *Adv. Mater.* **28** 2931–8
- [16] Yang X, Kong X T, Bai B, Li Z, Hu H, Qiu X and Dai Q 2015 Substrate phonon-mediated plasmon hybridization in coplanar graphene nanostructures for broadband plasmonic circuits *Small* **11** 591–6
- [17] Hu H, Zhai F, Hu D, Li Z, Bai B, Yang X and Dai Q 2015 Broadly tunable graphene plasmons using an ion-gel top gate with low control voltage *Nanoscale* **7** 19493–500
- [18] Zhao X, Yuan C, Zhu L and Yao J 2016 Graphene-based tunable terahertz plasmon-induced transparency metamaterial *Nanoscale* **8** 15273–80
- [19] Ke S, Wang B, Huang H, Long H, Wang K and Lu P 2015 Plasmonic absorption enhancement in periodic cross-shaped graphene arrays *Opt. Express* **23** 8888–900
- [20] Thongrattanasiri S, Koppens F H and Garcia de Abajo F J 2012 Complete optical absorption in periodically patterned graphene *Phys. Rev. Lett.* **108** 047401
- [21] Kim S, Jang M S, Brar V W, Tolstova Y, Mauser K W and Atwater H A 2016 Electronically tunable extraordinary optical transmission in graphene plasmonic ribbons coupled to subwavelength metallic slit arrays *Nat. Commun.* **7** 12323
- [22] Yao Y, Shankar R, Kats M A, Song Y, Kong J, Loncar M and Capasso F 2014 Electrically tunable metasurface perfect absorbers for ultrathin mid-infrared optical modulators *Nano Lett.* **14** 6526–32
- [23] Cai Y, Zhu J and Liu Q H 2015 Tunable enhanced optical absorption of graphene using plasmonic perfect absorbers *Appl. Phys. Lett.* **106** 043105
- [24] Song S, Chen Q, Jin L and Sun F 2013 Great light absorption enhancement in a graphene photodetector integrated with a metamaterial perfect absorber *Nanoscale* **5** 9615–9
- [25] Jang M S, Brar V W, Sherrott M C, Lopez J J, Kim L, Kim S, Choi M and Atwater H A 2014 Tunable large resonant absorption in a midinfrared graphene Salisbury screen *Phys. Rev. B* **90** 165409
- [26] Neubrech F, Pucci A, Cornelius T W, Karim S, Garcia-Etxarri A and Aizpurua J 2008 Resonant plasmonic and vibrational coupling in a tailored nanoantenna for infrared detection *Phys. Rev. Lett.* **101** 157403
- [27] Ayas S, Bakan G, Ozgur E, Celebi K and Dana A 2016 Universal infrared absorption spectroscopy using uniform electromagnetic enhancement *ACS Photonics* **3** 337–42
- [28] Abb M, Wang Y, Papasimakis N, de Groot C H and Muskens O L 2014 Surface-enhanced infrared spectroscopy using metal oxide plasmonic antenna arrays *Nano Lett.* **14** 346–52
- [29] Simsek E 2013 A closed-form approximate expression for the optical conductivity of graphene *Opt. Lett.* **38** 1437–9
- [30] Wang B, Zhang X, Yuan X and Teng J 2012 Optical coupling of surface plasmons between graphene sheets *Appl. Phys. Lett.* **100** 131111
- [31] Kong X T, Yang X, Li Z, Dai Q and Qiu X 2014 Plasmonic extinction of gated graphene nanoribbon array analyzed by a scaled uniform Fermi level *Opt. Lett.* **39** 1345–8
- [32] Guo X, Hu H, Zhu X, Yang X and Dai Q 2017 Higher order Fano graphene metamaterials for nanoscale optical sensing *Nanoscale* **9** 14998–5004
- [33] Hou H, Teng J, Palacios T and Chua S 2016 Edge plasmons and cut-off behavior of graphene nano-ribbon waveguides *Opt. Commun.* **370** 226–30
- [34] Rodrigo D, Tittl A, Limaj O, Abajo F J G D, Pruneri V and Altug H 2017 Double-layer graphene for enhanced tunable infrared plasmonics *Light: Sci. Appl.* **6** e16277
- [35] García de Abajo F J 2014 Graphene plasmonics: challenges and opportunities *ACS Photonics* **1** 135–52
- [36] Christensen J, Manjavacas A, Thongrattanasiri S, Koppens F H and Garcia de Abajo F J 2011 Graphene plasmon waveguiding and hybridization in individual and paired nanoribbons *ACS Nano* **6** 431–40
- [37] Liu N, Langguth L, Weiss T, Kastel J, Fleischhauer M, Pfau T and Giessen H 2009 Plasmonic analogue of electromagnetically induced transparency at the Drude damping limit *Nat. Mater.* **8** 758–62
- [38] Wu C, Khanikaev A B, Adato R, Arju N, Yanik A A, Altug H and Shvets G 2011 Fano-resonant asymmetric metamaterials for ultrasensitive spectroscopy and identification of molecular monolayers *Nat. Mater.* **11** 69–75
- [39] Zhao B and Zhang Z M 2015 Strong plasmonic coupling between graphene ribbon array and metal gratings *ACS Photonics* **2** 1611–8
- [40] Zhao B, Zhao J M and Zhang Z M 2014 Enhancement of near-infrared absorption in graphene with metal gratings *Appl. Phys. Lett.* **105** 031905
- [41] Zuloaga J, Prodan E and Nordlander P 2010 Quantum plasmonics: optical properties and tunability of metallic nanorods *ACS Nano* **4** 5269–76
- [42] Thongrattanasiri S, Manjavacas A and García de Abajo F J 2012 Quantum finite-size effects in graphene plasmons *ACS Nano* **6** 1766–75
- [43] Le F, Brandl D W, Urzhumov Y A, Wang H, Kundu J, Halas N J, Aizpurua J and Nordlander P 2008 Metallic nanoparticle arrays: a common substrate for both surface-enhanced Raman scattering and surface-enhanced infrared absorption *ACS Nano* **2** 707–18
- [44] Liu F and Cubukcu E 2013 Tunable omnidirectional strong light-matter interactions mediated by graphene surface plasmons *Phys. Rev. B* **88** 115439
- [45] Marini A, Silveiro I and Garcia de Abajo F J 2015 Molecular sensing with tunable graphene plasmons *ACS Photonics* **2** 876–82